



저작자표시-비영리-변경금지 2.0 대한민국

이용자는 아래의 조건을 따르는 경우에 한하여 자유롭게

- 이 저작물을 복제, 배포, 전송, 전시, 공연 및 방송할 수 있습니다.

다음과 같은 조건을 따라야 합니다:



저작자표시. 귀하는 원저작자를 표시하여야 합니다.



비영리. 귀하는 이 저작물을 영리 목적으로 이용할 수 없습니다.



변경금지. 귀하는 이 저작물을 개작, 변형 또는 가공할 수 없습니다.

- 귀하는, 이 저작물의 재이용이나 배포의 경우, 이 저작물에 적용된 이용허락조건을 명확하게 나타내어야 합니다.
- 저작권자로부터 별도의 허가를 받으면 이러한 조건들은 적용되지 않습니다.

저작권법에 따른 이용자의 권리는 위의 내용에 의하여 영향을 받지 않습니다.

이것은 [이용허락규약\(Legal Code\)](#)을 이해하기 쉽게 요약한 것입니다.

[Disclaimer](#)

공학석사 학위논문

Measurement of Temperature and Concentration  
Distributions for High-Temperature Gas  
by Using CT-TDLAS



지도교수 도 덕 희

2019년 2월

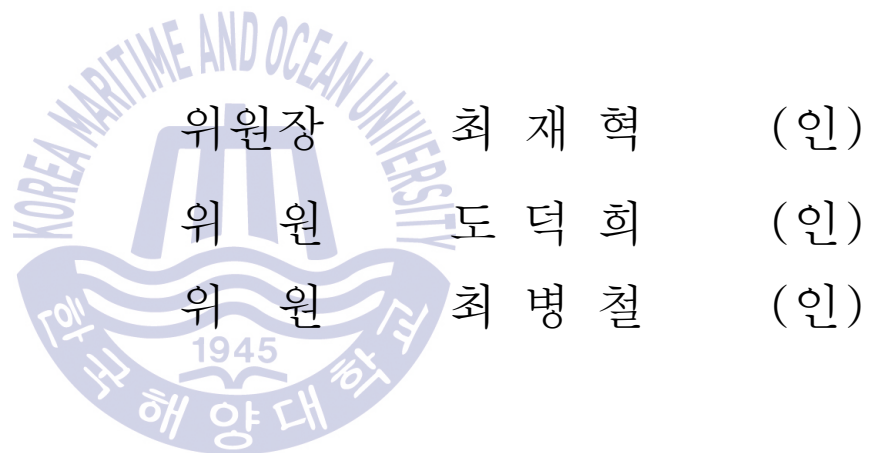
한국해양대학교 해양과학기술전문대학원

해양과학기술융합학과

김 준 호

<인준지>

본 논문을 김준호의 공학석사 학위논문으로 인준함.



2018년 12월 28일

한국해양대학교 해양과학기술전문대학원

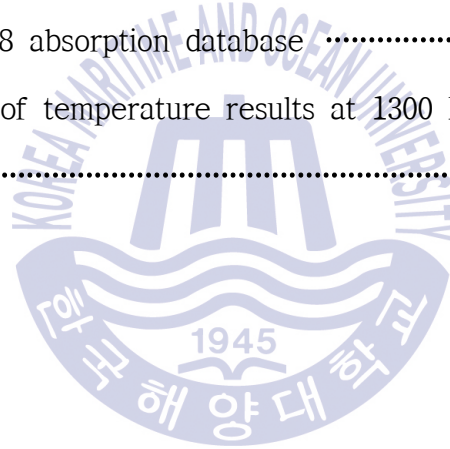
# Contents

List of Table .....	I
List of Figures .....	II
Nomenclature .....	VI
Abstract .....	VII
1. Introduction and Motivation .....	1
1.1 Introduction .....	1
1.2 Overview of thesis .....	4
2. Theoretical Background .....	5
2.1 A diode laser .....	5
2.2 Lambert-Beer' s law .....	9
2.3 Line strength .....	11
2.4 Line broadening function .....	15
2.5 Tomographic reconstruction algorithm .....	18
2.5.1 SMART method .....	21

<b>3. Experimental Details</b> .....	23
3.1 Experimental method .....	23
3.2 Data analysis .....	30
3.2.1 Initial treatment for absorption spectroscopy .....	30
3.2.2 Data process .....	33
<b>4. Results and Discussion</b> .....	35
4.1 Comparison performance of CT-TDLAS to thermocouple .....	35
4.2 Two-dimensional results using CT-TDLAS .....	40
<b>5. Conclusions</b> .....	47
5.1 Summary .....	47
5.2 Future works .....	48
<b>References</b> .....	49
<b>Acknowledgement</b> .....	55

## List of Tables

Table 2.1 Coefficients of the polynomial expression for the partition of H <sub>2</sub> O .....	14
Table 3.1 Experimental parameters for the combustion at each temperature	26
Table 3.2 Experimental conditions of the laser oscillation at ambient air ...	27
Table 3.3 HITRAN 2008 absorption database .....	32
Table 3.4 Comparison of temperature results at 1300 K, 1400 K and 1500 K .....	42



## List of Figures

Figure 2.1	Simplified single diode laser	7
Figure 2.2	Lattice constant and band gap energy of several semiconductors	8
Figure 2.3	The schematic diagram of Lambert-Beer's law	10
Figure 2.4	Boltzmann distribution for different temperature range	14
Figure 2.5	Analysis grid and laser beam path	20
Figure 2.6	Flow chart of pattern matching algorithm	22
Figure 3.1	The schematic of the CT-TDLAS system for two-dimensional thermometry	25
Figure 3.2	The measurement cell	28
Figure 3.3	Thermocouple (B-type) for validation	29
Figure 3.4	Measurements spots using the thermocouples (R and B-Type)	29
Figure 3.5	H <sub>2</sub> O absorption spectra of each temperature (300 K, 700 K, 1200 K, 1500 K) at 1395.4 nm ~ 1395.8nm	31
Figure 3.6	Temperature dependence of two absorption lines	31
Figure 3.7	The absorption spectrum of line number 4 measured at 1200 K	34
Figure 3.8	An example of absorption line and the baseline fit	34
Figure 4.1	The absorption lines at 300 K	37
Figure 4.2	The absorption spectra at 300 K 64 points	37

Figure 4.3	The averaged absorption lines at 1300 K .....	38
Figure 4.4	The absorption spectra at 1300 K .....	38
Figure 4.5	Comparison of temperature results .....	39
Figure 4.6	Comparison of the temperature results I .....	41
Figure 4.7	Comparison of the temperature results II .....	42
Figure 4.8	Temperature fields by CT-TDLAS .....	44
Figure 4.9	Concentration fields by CT-TDLAS .....	46



## 사용 기호

### Nomenclature

$I_0$	Incident light intensity
$I_t$	Transmitted light intensity
$a_\lambda$	Absorbance
$n_i$	Number of density of species 'i'
$P$	Pressure
$L$	Length of laser beam path
$S_{i,j}$	Temperature dependent absorption line strength of the absorption line 'j'
$G_{vi,j}$	Light line broadening function of line shape function
$E''$	Lower state energy level
$Q(T)$	Partition function
$h$	Plank's constant( $h=6.6256 \cdot 10^{-27}$ [erg · s])
$k$	Boltzmann's constant( $6.6256 \cdot 10^{-27}$ [erg/K])
$c$	Light speed( $3.0 \cdot 10^{10}$ [cm/s])
$\nu_0$	Wavenumber
$A$	The amount of absorption
$\beta$	Relaxation parameter
$T$	Temperature [K]

# Measurement of Temperature and Concentration Distributions for High-Temperature Gas by Using CT-TDLAS

by Joon Ho KIM

*Department of the Convergence Study on the Ocean Science and  
Technology  
Graduate School of Korea Maritime and Ocean University*



Abstract

This thesis is mainly focused on the measurements of the temperature and concentration fields of a high pure propane( $C_3H_8$ ) gas. The temperature and concentration fields were measured by utilizing the laser absorption characteristics.

In order to measure the temperature and concentration fields, an optical tomograph measurement system has been constructed, in which laser technology and tomography technology were adopted.

The optical signals were obtained from the laser signals that had been passed through the combustion field of the propane gas, and these were used for reconstructing the temperature and concentration field.

TDLAS (tuneable diode laser absorption spectroscopy) principle has been adopted, in which the intensity of the laser passed through the combustion field is absorbed according to the concentration of the gas molecule. The concentration field has been measured by adopting the tomography technology.

The present measurement system, optical tomography system, constructed in this thesis is capable of measuring the temperature and concentration fields up to 1500 K.

To attain this goal, two key approaches had been adopted. Firstly, an auto profiling method has been constructed, which is capable of reconstructing very weak signals at the wavelength of 1395.2–1395.8 nm of laser. Secondly, the SMART (Simultaneous Multiple Algebraic Reconstruction Technique) algorithm has been adopted.

The temperature field measured by the constructed optical tomography was compared with those measured by thermocouples (B&R type), through which it was confirmed that the measurement discrepancy between them was within 7 %.

# CT-TDLAS를 이용한 고온 가스의 온도·농도 분포 산정에 관한 연구

김 준 호

한국해양대학교 해양과학기술전문대학원

해양과학기술융합학과

초록

본 논문은 고순도 Propane ( $C_3H_8$ )을 연료로 한 연소 시 발생하는 가스의 온도, 농도 측정에 관한 연구내용을 담고 있다. 가스의 온도와 농도분포는 수증기( $H_2O$ )의 레이저흡수특성을 이용하였다.

온도장과 농도장 측정을 위하여 레이저기술과 토모그래피(tomography) 기술을 접목시킨 광학-토모그래피 측정시스템을 완성하였다. 고순도 프로판 가스의 연소장을 통과한 광학신호를 이용하여 온도와 농도장을 재구성하였다.

반도체 레이저로부터 나오는 빛이 가스분자의 농도에 따라 흡수되는 특성을 이용한 레이저 흡수법(TDLAS, tuneable diode laser absorption spectroscopy)을 적용하였고, 공간상에서의 농도분포를 측정하기 위하여서

는 토모그래피 기술을 융합 접목하였다.

본 논문에 구현된 ‘광학-토모그래피 측정시스템’은 가스온도가 1500 K까지 농도분포를 측정할 수 있는 시스템이다.

이를 달성하기 위하여, 두 가지 핵심기술을 완성 적용하였다. 첫째, 고온부에서 반응하는 반도체레이저 파장(1395.2-1395.8 nm 파장대)에서 미약한 광학신호를 재구성할 수 있는 자동프로파일링 기술(auto profiling)을 적용하였으며, 둘째, 가스의 농도와 온도 분포를 동시에 측정할 수 있는 SMART 알고리즘 (Simultaneous Multiple Algebraic Reconstruction Technique)을 완성 적용하였다.

측정된 온도 값에 대한 검증을 위하여 열전대(B&R type)를 이용한 온도 측정값과 본 연구에서 개발한 ‘광학-토모그래피 측정시스템’에 의한 온도 측정값을 비교한 결과, 측정 온도차이가 7 % 미만으로 나타났으며, 농도분포 측정에서의 상대오차도 동일한 수준으로 측정할 수 있음이 확인되었다.

# Chapter 1 Introduction and Motivation

## 1.1 Backgrounds

As global warming issues become more socially appealing globally, efforts to reduce greenhouse gases, which are the most important factors of global warming, are actively underway. Starting with the Rio Summit, the first international treaty on climate change, in 1992, the Kyoto protocol and the Paris Accord, which were adopted in 1997 and 2015, respectively, have become a standard international convention on climate change. Also, the International Maritime Organization (IMO), one of the specialized agencies of the United Nations, is tightening regulations each year to reduce pollutant emissions. All vessels built after 2013 in accordance with MARPOL has to be issued with the IEE (International Energy Efficiency) from Classification Society. According to Regulation 14 in Annex VI of the International Convention for the Prevention of Pollution from Ships, since 2020, in an effort to reduce SO<sub>x</sub> emissions, a sulfur content limit of 0.5 % or less in all fuel oil will be applied globally (J.H. Kim et al, 2018).

In this context, the needs of a precise measuring technique for emission gas are growing. Recently, many researches of non-contact and laser-based measuring systems such as Spontaneous Raman Spectroscopy,

CARS: Coherent Anti-Stokes Raman Spectroscopy (Ax et al. 2010; Braeuer and Leipertz 2009; Jehlickan et al., 2009), LIF: Laser-Induced Fluorescence (Engel et al., 2009), TDLAS: Tunable Diode Laser Absorption Spectroscopy (L. Xiang et al., 2006) and LIBS: Laser-Induced Breakdown Spectroscopy (H. Hou et al., 2014) have been presented and developed. However, these techniques showed some limitations in measuring light intensity changes due to temperature and pressure, and detecting multiple components in emission gas.

In the case of TDLAS, another laser diagnostic, which uses the absorption phenomena to measure species temperature and species concentration, it is combined with CT (Computed Tomography), which is widely used in the medical fields so as to break through these limits (Deguchi et al.; 2012).

Additionally, for obtaining higher spatial resolution, Yoon et al. (2018) and Jeon et al. (2018) proposed an improved CT-TDLAS system which provided three-dimensional temperature and concentration fields in combustion flows (especially, Jeon mixed two diode lasers near 1343 nm, 1388 nm). However, these researches also had some errors (about 30% at 700 K) at high temperature flows, and using two diode lasers required higher cost and more complicated optical facility. Moreover, only restricted temperature range (300 K - 800 K) could be allowed to measure.

In this paper, to increase accuracy of temperature evaluation at high temperature and to expand the measuring range till 1500 K, an improved CT-TDLAS system using single diode laser (1395 nm) is introduced.



## 1.2 Overview of thesis

The work presented in this thesis aims to extend the measurement capabilities of the CT-TDLAS for high temperature combustion non-uniform flows. The results is an comprehensive database of measurements that help to the combustion and measurement research fields. The dissertation is organized as follows.

In chapter 1, the usage of laser application measurement and its motivation are introduced. Chapter 2 describes fundamental theory used in laser absorption spectroscopy sensors, and reconstruction algorithm for higher spatial resolution is presented. Chapter 3 contains experimental details and the process of converting absorption to measurements of two-dimensional temperature and concentration is examined. In chapter 4, the results of this experiment are reported, and it is validated with thermocouple (B-type), comparing each result. Finally, chapter 5 summarizes the development of CT-TDLAS and results of this thesis and presents possible avenues for future work.

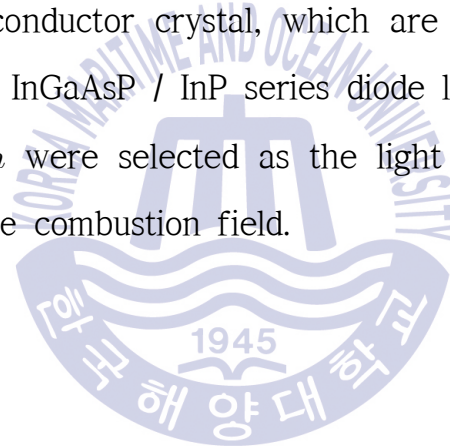
## Chapter 2 Theoretical Background

### 2.1 A diode laser

A Diode laser collectively refers to the generators and amplifiers of light waves using induction discharge of tubes by the optical stream of electrons in a semiconductor. A diode laser is the smallest and lightest among laser and has the advantage of being mass-produced at low cost through semiconductor process.

A diode lasers is electrically a PIN diode that compounds semiconductors such as InP and GaAs, as shown in Fig. 2.1. On top and bottom of semiconductor are electrodes with positive and negative cathode. The basic conditions for the laser oscillation are a resonant mirror, an active medium, and an excitation source. In the case of a diode laser, the forward bias is an excitation source, and the cleaved surface itself, which is caused by the difference in refractive index between the semiconductor facing each other and the air layer formed therebetween, is used as a reflecting mirror, and then resonance occurs between the bonding surfaces. The photon energy emitted by the semiconductor diode laser is equal to the band-gap energy of the

semiconductor material. Therefore, a semiconductor material with a direct transitional band-gap in the desired wavelength must be selected. The oscillation wavelength  $\lambda$  of a diode laser with direct band gap semiconductors is determined by the band gap energy  $E_g$  and has an  $\lambda[\mu m] = 1.2398/E_g$  relationship. Fig.2.2 shows the relationship between the band-gap energy of the major semiconductor and the lattice constant of the semiconductor crystal, which are widely used as optical devices. In this study, InGaAsP / InP series diode lasers with wavelengths of 1.3  $\mu m$  and 1.5  $\mu m$  were selected as the light sources for measuring the water vapor in the combustion field.



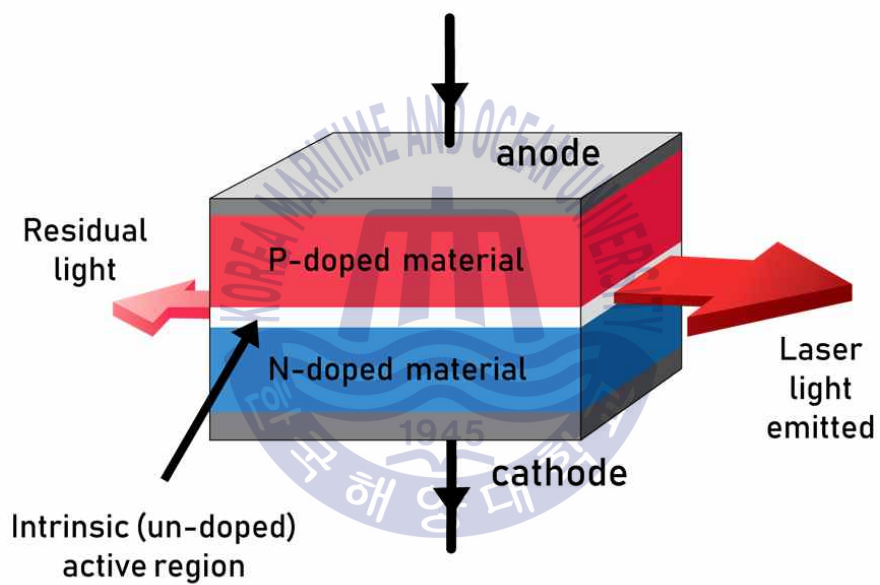


Fig. 2.1 Simplified single diode laser

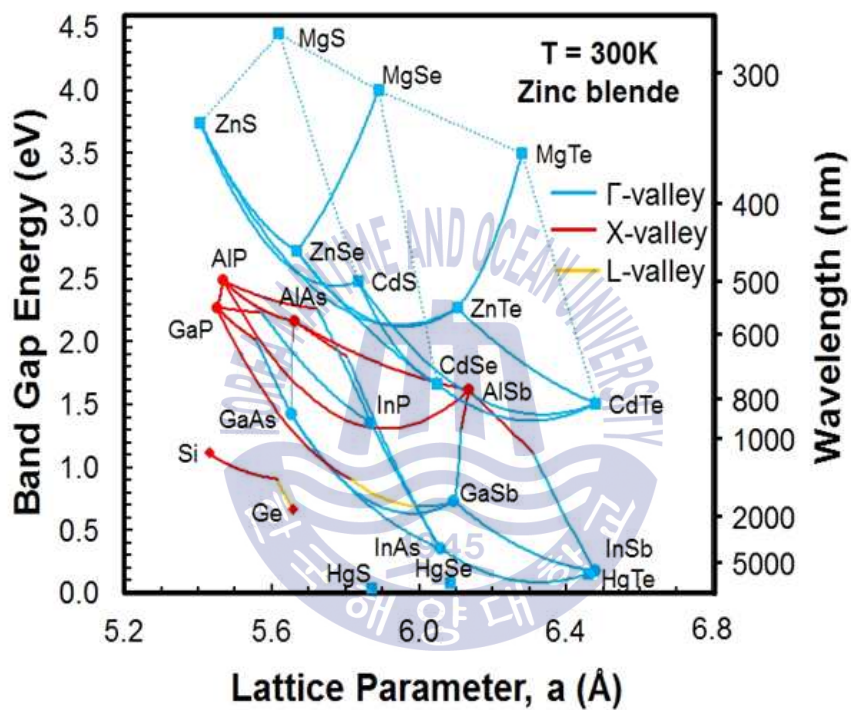


Fig. 2.2 Lattice constant and band gap energy of several semiconductors

## 2.2 Lambert-Beer' s law

TDLAS (Tunable Diode Laser Absorption Spectroscopy) is a technique that uses absorption phenomena to measure species temperature and concentration. As Fig. 2.3 depicts, when the incident laser beam permeates a absorption medium, the concentration of the molecules is proportional to the transmitted intensity of the light according to the Lambert-Beer' s law (D.F. Swinehart; 1962). The molecular concentration relates to the amount of absorbed light, as in the following Eq. (2.1):

$$\frac{I_t(\lambda)}{I_0(\lambda)} = \exp\{A_\lambda\} = \exp\left\{-\sum_i (P \cdot n_i \cdot L \sum_j S_{i,j}(T) G_{\nu_i,j})\right\} \quad (2.1)$$

Here,  $I_0$  is the incident light intensity,  $I_t$  is the transmitted light intensity,  $A_\lambda$  is the absorbance,  $P$  is the pressure,  $n_i$  is the number density of species  $i$ ,  $L$  is the path length,  $S_{i,j}$  is the temperature dependent absorption line strength of the absorption line  $j$ , and  $G_{\nu_i,j}$  is the line broadening function.

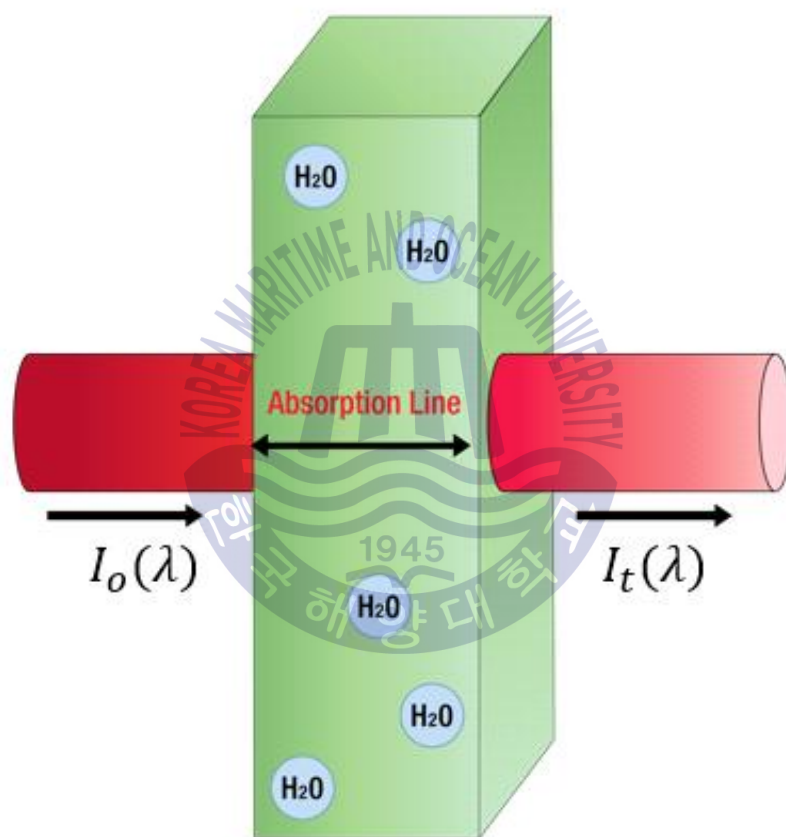


Fig. 2.3 The schematic diagram of Lambert-Beer's law

## 2.3 Line-strength

Line-strength a function of the temperature, and it is expressed by pressure dependent  $S[cm^{-2}atm^{-1}]$ , and  $S^*[cm^{-1}/mol \cdot cm^{-2}]$ , which is a unit of number density by HITRAN(High resolution Transmission) for each molecule evaluated that Harvard-Smithsonian Center for Astrophysics, Cambridge MA, USA provides. Eq. (2.2) shows a function of line-strength.

$$S[cm^{-2}atm^{-1}] = \frac{S^*[cm^{-1}/mol \cdot cm^{-2}] \times n[molecules/cc]}{P[atm]} \quad (2.2)$$

Here,  $n$  is the number density[molecules/cc], and  $P$  is pressure[atm](L.S. Rothman et al; 2005). The number density,  $n$ , is expressed as in the following Eq. (2.3), and then, Eq. (2.5) can be formulated as ideal gas equation. Eq. (2.4) is applied to Eq. (2.2).

$$n = \frac{N}{V} \quad (2.3)$$

$$PV = NkT \quad (2.4)$$

$$S[atm^{-2}atm^{-1}] = \frac{S^*[cm^{-1}/mol \cdot cm^{-2}] \times 1013250[dynes/(cm^2 \cdot atm)]}{kT} \quad (2.5)$$

Here,  $k$  [J/K] is Boltzmann's constant, and  $T$  [K] is temperature of the target gas. Applying Boltzmann's Constant to Eq. (2.5), Eq. (2.6) is derived, and then as  $T$  is considered as Room temperature, 296 K, Eq. (2.7) can be expressed.

$$S = \frac{S^* \times (7.34 \times 10^{21})}{T} [cm^{-2} atm^{-1}] \quad (2.6)$$

$$S = S^* \times (2.488 \times 10^{19}) [cm^{-2} atm^{-1}] \quad (2.7)$$

The line strength in the state of gas molecules absorbing light is described as a Boltzmann distribution and the Boltzmann distribution is temperature-dependent as shown in Fig. 2.4, so that the line strength is a function of temperature. It can be explained as the following Eq. (2.8).

$$S_v(T) = S_v(T_0) \frac{T}{T_0} \frac{Q(T_0)}{Q(T)} \exp \left[ - \frac{hcE_i''}{k} \left( \frac{1}{T} - \frac{1}{T_0} \right) \right] \left[ \frac{1 - \exp \left( \frac{-hcV_{0,v}}{kT} \right)}{1 - \exp \left( \frac{-hcV_{0,v}}{kT_0} \right)} \right] \quad (2.8)$$

Here,  $h$  is Planck's constant ( $6.6256 \cdot 10^{-27}$  [J · s]),  $k$  is Boltzmann's constant ( $k=1.38054 \cdot 10^{-16}$  [erg/K]),  $Q(T)$  is the partition function of the

absorbing molecule,  $T_0$  is the reference temperature (usually 296 K),  $c$  is the speed of light ( $3.0 \cdot 10^{10}$ [cm/s]),  $\nu_0$ [ $\text{cm}^{-1}$ ] is the line-center frequency and  $E'$ [ $\text{cm}^{-1}$ ] is the lower state energy of the transition. The lower state energy  $E'$  determines the equilibrium molecular population in the non-absorbing state as a function of temperature, and thus controls how the line-strength of a particular transition varies with temperature. Additionally, the temperature-dependent partition function which relates to the quantity of molecular energy is expressed as the following Eq. (2.9).

$$Q(T) = a + bT + cT^2 + dT^3 \quad (2.9)$$

Here, the coefficients,  $a$ ,  $b$ ,  $c$ , and  $d$  are in tables 2.1 as below and depend on the temperature interval.

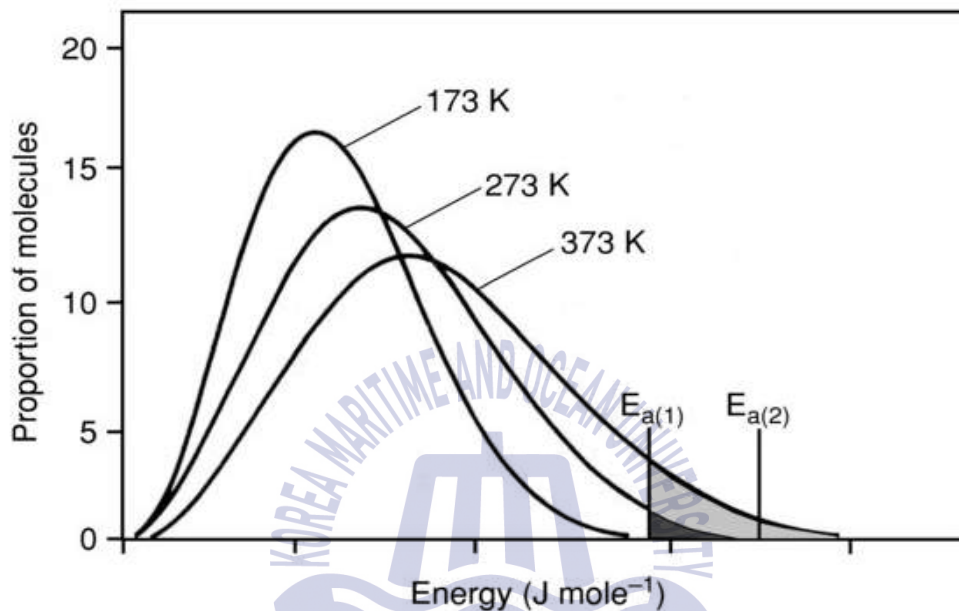


Fig.2.4 Boltzmann distribution for different temperature range (D.I. Yoon, 2018, master degree thesis)

Table 2.1 Coefficients of the polynomial expression for the partition of H<sub>2</sub>O

coefficients	70<T<500 K	500<T<1500 K	1500<T<3005 K
a	$-0.44405 \times 10^1$	$-0.94327 \times 10^2$	$-0.11727 \times 10^4$
b	$0.27678 \times 10^0$	$0.81903 \times 10^0$	$0.29261 \times 10^1$
c	$0.12536 \times 10^{-2}$	$0.74005 \times 10^{-4}$	$-0.13299 \times 10^{-2}$
d	$-0.48938 \times 10^{-6}$	$0.42437 \times 10^{-6}$	$0.74356 \times 10^{-6}$

## 2.4 Line broadening function

The line-shape function of a particular absorption transition, corresponding to the relative energy change in spectral absorption with frequency, is determined by the physical mechanism that confuses the energy level of the transfer or the way that the molecules in a target gas interact with the laser (Herzberg 1945, Yariv 1982, Banwell and McCash 1994). In this paper, the line-shape of the target transition is approximately fit by a Voigt profile, taking into account both the effect of Doppler Broadening and Collisional Broadening. Eq. (2.10) and (2.11) represent the Voigt profile (Th .H. de Keijser et al; 1982) .

$$G_V(V) = \int_{-\infty}^{\infty} G_D(u)G_C(V-u)du \quad (2.10)$$

$$G_V(V) = G_D \frac{a}{\pi} \int_{-\infty}^{\infty} \frac{\exp(-y^2)dy}{a^2 + (x-y)^2} = G_D(V_0) V(a,x) \quad (2.11)$$

Here,  $a$  indicates the relative influence of the line broadening caused by Doppler Broadening and Collisional Broadening, and as the broadening influence due to the collision increases, and  $a$  also increases, which can

be represented as shown in Equation (2.12).  $x$  is the distance of the dimensionless from the center of the absorption line, and is expressed by Eq. (2.13). The Doppler full-width at half maximum (FWHM),  $\Delta V_D [cm^{-1}]$ , is given by Eq. (2.14).

$$a = \frac{\sqrt{\ln 2} \Delta V_c}{\Delta V_D} \quad (2.12)$$

$$x = \frac{2\sqrt{\ln 2}(V - V_0)}{\Delta V_D} \quad (2.13)$$

$$\Delta V_D = V_0 \sqrt{\frac{8kT \ln 2}{mc^2}} \approx 7.1623 \times 10^{-7} V_0 \sqrt{\frac{T}{M}} \quad (2.14)$$

Here,  $M$  is the molecular weight of the absorbing species.  $G_C(V)$  and  $G_D(V)$  are expressed as the following Eq. (2.14) and (2.15) representing the Lorentz function and the function for the Doppler broadening (Y. Zaatar, et al., 2000) (P.J. Chantry et al, 1971).

$$G_C(V) = \frac{1}{\pi} \frac{\frac{\Delta V_c}{2}}{(V - V_0)^2 + \left(\frac{\Delta V_c}{2}\right)^2} \quad (2.14)$$

$$G_D(V) = \frac{2}{\Delta V_D} \sqrt{\frac{\ln 2}{\pi}} \exp -4 \ln 2 \left( \frac{V - V_0}{\Delta V_D} \right)^2 \quad (2.15)$$

Here,  $\Delta V_c [cm^{-1}]$  and  $V_0 [cm^{-1}]$  is collisional line width and line-center frequency, respectively, and  $\Delta V_c [cm^{-1}]$  is represented in the following Eq. (2.16).

$$\Delta V_c = P \sum_j (X_j 2\gamma_i) \quad (2.16)$$

The collision broadening depends on species concentration and temperature. In this study we assume total collisional broadening of the measured field and each species dependence on collisional broadening parameters is not considered. The collisional broadening parameters are determined by measured spectra (T. Kamimoto et al, 2015). The natural broadening is not considered since the influence of the natural broadening was neglected in this study.

## 2.5 Tomographic reconstruction algorithms for TDLAS

TDLAS, a line of sight measurement technique, has a limit in offering precise information over a section. In order to overcome it, CT (Computed Tomography), which is widely used in medical field was applied to TDLAS that provides two or three dimensional information over a section (F. Wang et al, 2010; Y. Deguchi, 2013). The ART (Algebraic Reconstruction Technique) method, which is a conventional reconstruction algorithm, has been used with a filtered back projection (FBP) method based on the Fourier domain. However, this technique uses a large amount of transmitted light, so it consumes too long time to reconstruct. To overcome this shortcoming, multiple reconstruction techniques such as MART (Multiplicative Algebraic Reconstruction Technique, SART (Simultaneous Algebraic Reconstruction Technique), SMART (Simultaneous Multiple Algebraic Reconstruction Technique) were devised (D. Verhoeven. 1993; A.H Andersen & A.C Kak. 1984; D.C Noll et al.. 1998). Jeon et al. (2014, 2017) has demonstrated that among these algorithm the SMART method proved to perform best in TDLAS system. In this paper, the SMART method was used to offer two dimensional information on water-vapour in combustion field.

In this paper, as Fig. 2.10 shows, with a set of laser beam, analysis grid for two dimensional information was formed. Then, using the absorption spectrum obtained from the experiment, theoretically reconstructs information on all laser intensities of the analysis region  $i$ . The absorption intensity in each laser beam path,  $j$ , is reconstructed by Eq. (2.16).

$$A_{\lambda,j} = - \sum_i n_i \cdot L_{i,j} \cdot \alpha_{\lambda,j} \quad (2.16)$$

Here,  $A_{\lambda,j}$  is the absorbance in laser beam,  $j$ ,  $\alpha_{\lambda,j}$  is the absorption coefficient.  $L_{i,j}$  is the length between each laser beam.

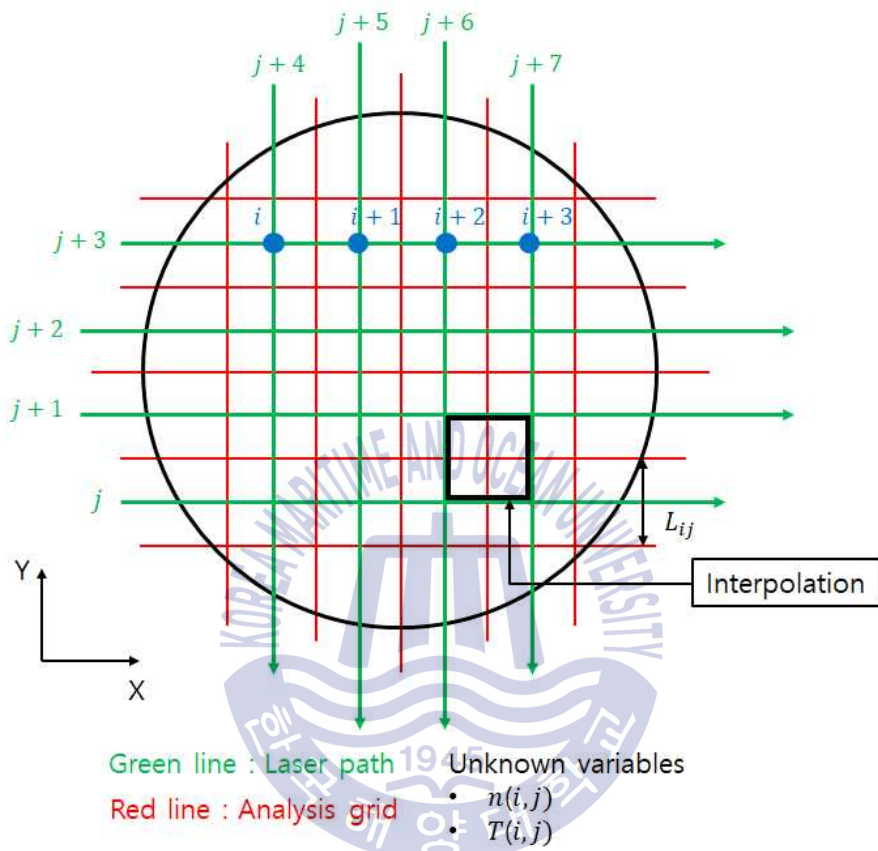


Fig. 2.10 Analysis grid and laser beam path

### 2.5.1 SMART method

The SMART method is a multiplication-based iterative computation algorithm, which is calculated repeatedly until the difference between the measured and presumed amount of absorption is minimized as the following Eq. (2.17).

$$\alpha_{\lambda,i}(i)^{k+1} = \alpha_{\lambda,j}(i)^{(k)} \times \sum_{i=1}^{N_i} \left[ \left( \frac{(A_{\lambda,j})_{\text{experiment}}}{\sum_{i=1}^i \alpha_n^k \cdot L_{i,j}} \right)^{\beta L_{i,j}} \right]^{1/N_i} \quad (2.17)$$

Here,  $i$  represents analytical grid, and  $j$  indicates laser path. The SMART method provides the temperature distribution with the minimum error through the flowchart as shown in Fig. 2.11.

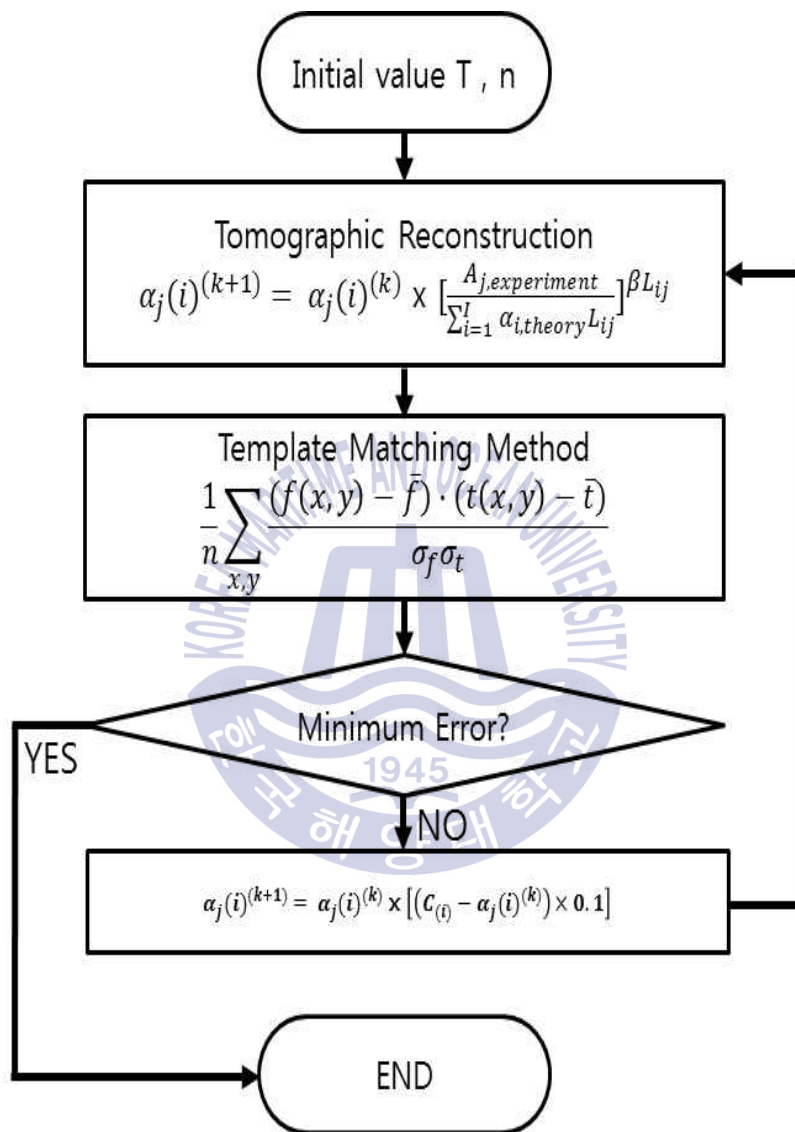


Fig. 2.11 Flow chart of pattern matching algorithm (D.I. Yoon, 2018, master degree thesis)

## Chapter 3 Experimental details

### 3.1 Experimental method

Fig. 3.1 depicted the schematic of CT-TDLAS system for measuring two-dimensional temperature and concentration fields of water-vapour generated in the combustion field. The flow of Dry-air (20.8 %, O<sub>2</sub>) and Propane (99.5 %, C<sub>3</sub>H<sub>8</sub>) which fueled the stable combustion were precisely controlled by mass meter (KOFLOC 7200) for each gas. Table 3.1 described the combustion parameters at each temperature.

In this paper, a laser diode (Santec, HSL-200-30-TD) was used to probe water-vapour absorption transition near 1395 nm. Adjusting the laser injection temperature and current, waveforms to scan the desired wavelength band were generated digitally from a function generator and a LD driver. With the scan rate described in Table 3.2, the laser beam was oscillated and then the combined signal was split onto 16 fibers by a fiber splitter (OPNETI CO., 1×16, 1310 nm SWBC). Collimators (THORLABS CO., 50-1310-APC) irradiate each beam into the measurement cell with 16 path. The transmitted signal across the combustion field was detected by 16 Photo-diodes (Hamamastu Photonics,

near  $1.3 \mu\text{m}$ ), and recorded in a memory hi-corder as a form of absorption line.

Fig. 3.2 showed the drawing of the measurement cell and its  $8 \times 8$  laser path. The diameter of the measurement cell and length between each laser beam was 90 mm and 15 mm respectively.

The temperature measurements using CT-TDLAS were carried out at 1300 K, 1400 K, & 1500 K respectively. When it comes to the measurements at 300 K, it was for obtaining calibration data, as earlier mentioned. To demonstrate the performance of CT-TDLAS, the temperature measurements with various sorts of thermocouples (B and R-Type, Heraeus, assembled by SE-KI) was carried out and its results were compared. A picture of measurement with the thermocouple was in Fig. 3.3. Since measurement in higher temperature (over 1300 K) with K-type had error, even though its temperature range was referenced up to 1500 K, B and R-type that is proper only for measuring at higher temperature were used instead. Measurements were carried out three times: two times at the location 4, and -4 according to laser beam path, and one at the location 0, near the flame. Measurement points using the thermocouples were depicted in Fig. 3.4.

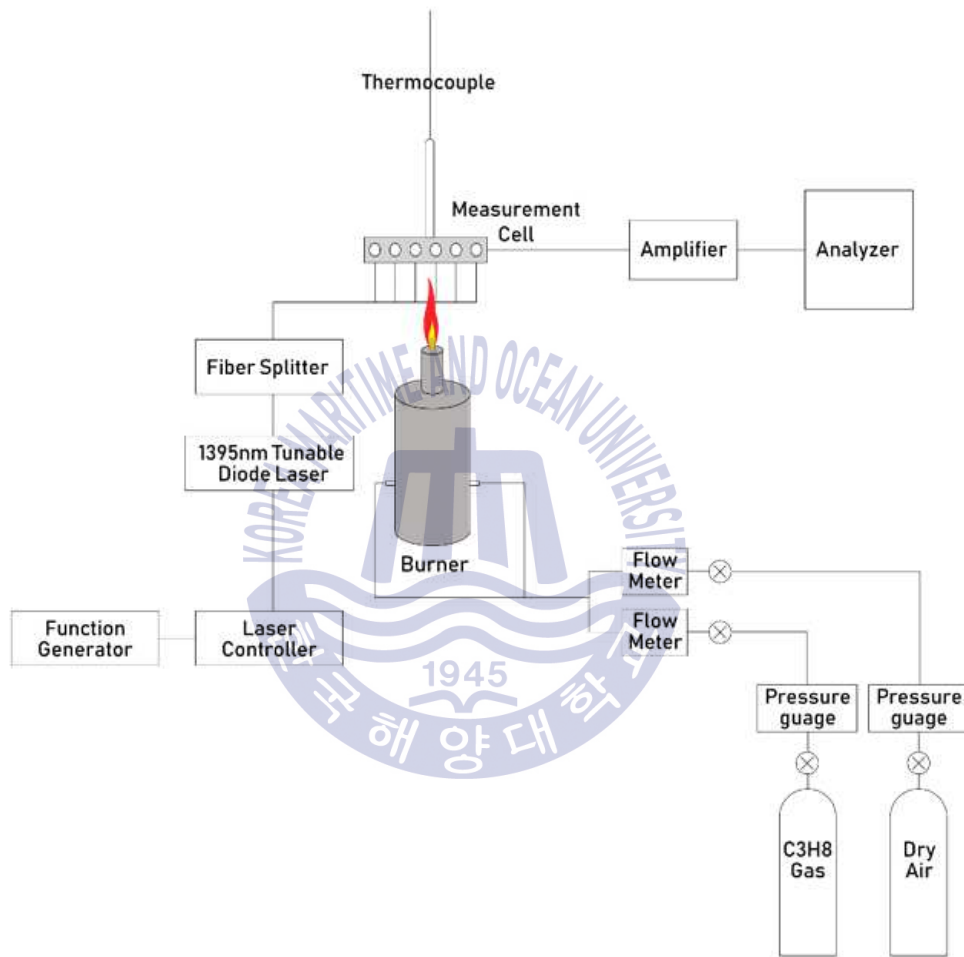


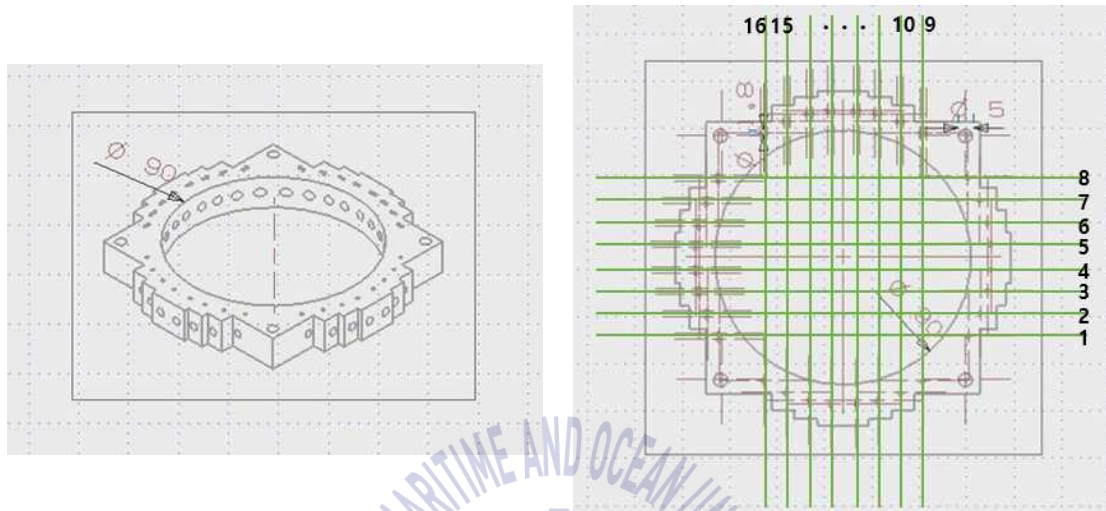
Fig. 3.1 The schematic of CT-TDLAS system for two-dimensional temperature measurement in a flame burner

**Table 3.1** Experimental parameters for the combustion at each temperature

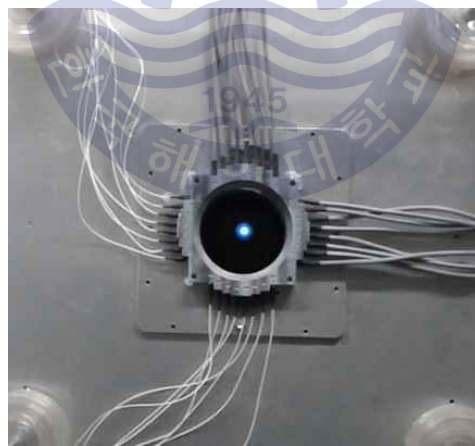
Case	Property (-)	Flow Rate (L/min)	Pressure (MPa)	Temperature at the flame
Cal.	-	-	-	(Room Temperature)
	-	-	-	300 K
1	Dry-Air	1.40	0.4	1300 K
	Propane	0.07	0.15	
2	Dry-Air	1.50	0.4	1400 K
	Propane	0.08	0.15	
3	Dry-Air	3.20	0.4	1500 K
	Propane	0.15	0.15	

**Table 3.2** Experimental conditions of the laser oscillation at ambient air

used laser	
near 1395 nm	
Laser Controller	
temperature	15.7 °C
current	162.01 mA
Function Generator	
frequency	1 kHz
amplitude	4.3 V
offset	1.6 V
wave shape	saw tooth
Memory hi-corder	
sampling rate	2 $\mu$ s
measuring time	1 s



(a) The drawing of the measurement cell



(b) An actual measurement cell

Fig. 3.2 Measurement cell

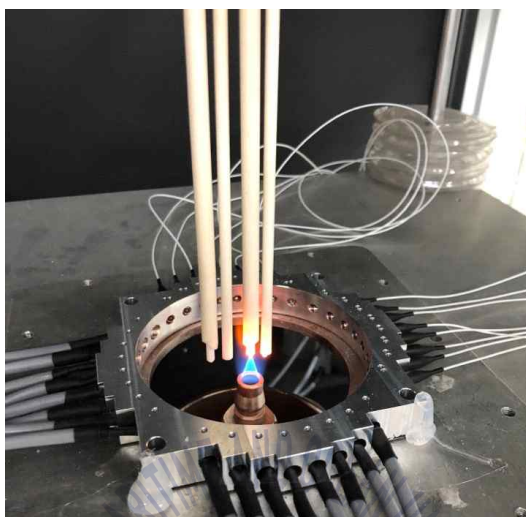


Fig. 3.3 Thermocouple (B-type) for validation

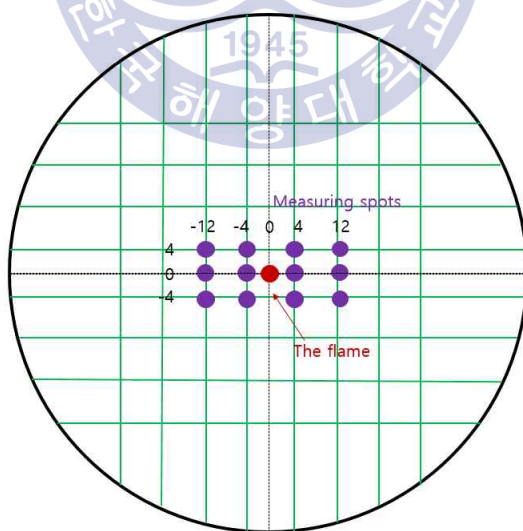


Fig. 3.4 Measurements spots using the thermocouples (R and B-Type)

## 3.2 Data analysis

### 3.2.1 Initial treatment for absorption spectroscopy

In this work, a diode laser near 1395 nm for measurements of temperature and concentration of water-vapour during combustion was used. As shown in Fig. 3.5, in near 1395 nm, near-infrared ray, theoretical absorption spectra of water-vapour which was shaped by Voigt profile which provide the integrated absorbance  $A$ , and collisional FWHM  $\Delta\nu_c$  from which the line strength  $S(T)$ , and broadening coefficients are calculated at each temperature (300 K, 700 K, 1200 K & 1500 K) were pictured (L.S. Rothman et al.; 2009). In Fig. 2.8, around 1395.51 nm and 1395.69 nm, the relative intensities significantly depended on the temperature, so that it was utilized for evaluation of temperature in a way of calculating temperature using the ratio of peak points. The relative intensities of the representative wavelength were compared in accordance with varying temperature, which was illustrated in Fig. 3.6, and it was figured out that over 900 K the temperature could be comparably evaluated, meaning the diode laser of 1395 nm was proper for high temperature measurements. In Table 3.3, parameters that HITRAN database provided were (E.E. Whiting; 1968).

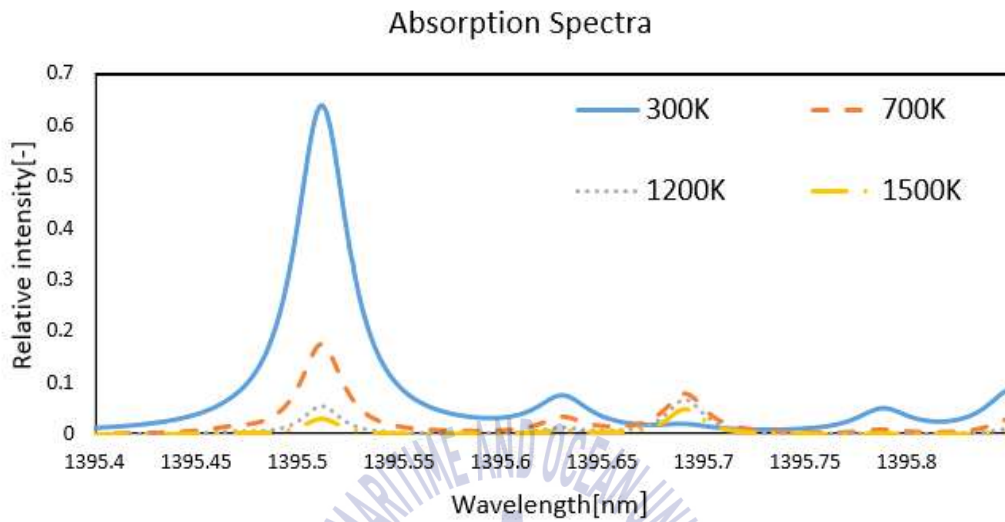


Fig. 3.5 H<sub>2</sub>O absorption spectra of each temperature (300 K, 700 K, 1200 K, 1500 K) at 1395.4 nm ~ 1395.8nm

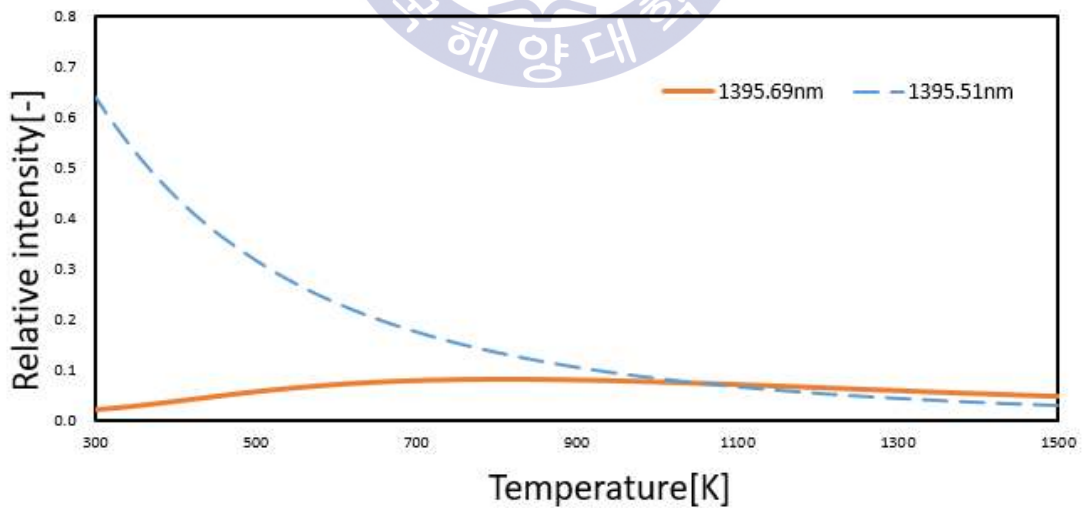


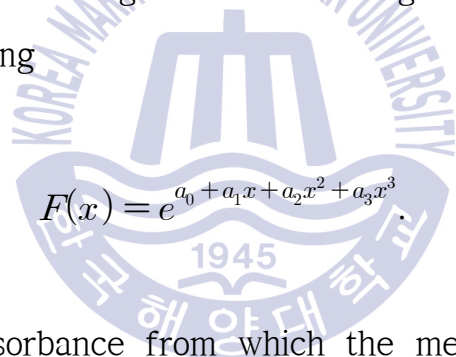
Fig. 3.6 Temperature dependence of two absorption lines

Table 3.3 HITRAN 2008 absorption database

Wave Number [cm <sup>-1</sup> ]	Wavelength [nm]	Line-strength [cm <sup>-1</sup> · atm <sup>-1</sup> ]	E'' [cm <sup>-1</sup> ]
7164.708	1395.73	2.10E-06	1282.919
7164.731	1395.73	3.96E-09	1690.664
7164.891	1395.69	8.51E-08	2053.969
7164.902	1395.69	9.48E-04	1394.814
7164.903	1395.69	2.85E-03	1394.814
7164.983	1395.68	3.51E-08	2433.799
7165.098	1395.65	1.96E-04	1131.776
7165.140	1395.65	2.32E-07	704.214
7165.170	1395.64	2.40E-08	2927.074
7165.215	1395.63	1.57E-02	399.4575
7165.266	1395.62	2.38E-05	1664.965
7165.407	1395.59	5.56E-08	3316.145
7165.510	1395.57	1.04E-05	1033.195
7165.511	1395.57	4.08E-05	1033.194
7165.512	1395.57	4.96E-09	2462.875
7165.693	1395.54	2.20E-07	1574.678
7165.754	1395.53	7.30E-08	1574.678
7165.776	1395.52	1.26E-08	2613.104
7165.821	1395.51	1.44E-01	212.1564
7166.051	1395.47	6.31E-04	1050.158
7166.067	1395.47	7.13E-09	1767.339

### 3.2.2 Data process

The acquired absorption spectrum of water-vapour of fig 3.7 generated from the combustion field at 1200 K was obtained by the following procedure (Only line number 4 of the 16 lines was depicted for convenience). Firstly, to reduce white noise, 50 spectrum cycles of water-vapour were averaged, and a baseline (red colored line in Fig. 3.8) was fitted to the target transition region with the 3rd-order exponential curve fitting


$$F(x) = e^{a_0 + a_1x + a_2x^2 + a_3x^3} \quad (3.1)$$

Then, the single absorbance from which the measured absorption line subtracted from the baseline fit, compared to the corresponding absorbance spectrum taken from HITRAN 2008. With these processes, the absorption spectra for 16 laser path were ascertained (L. Dong, et al. 2016).

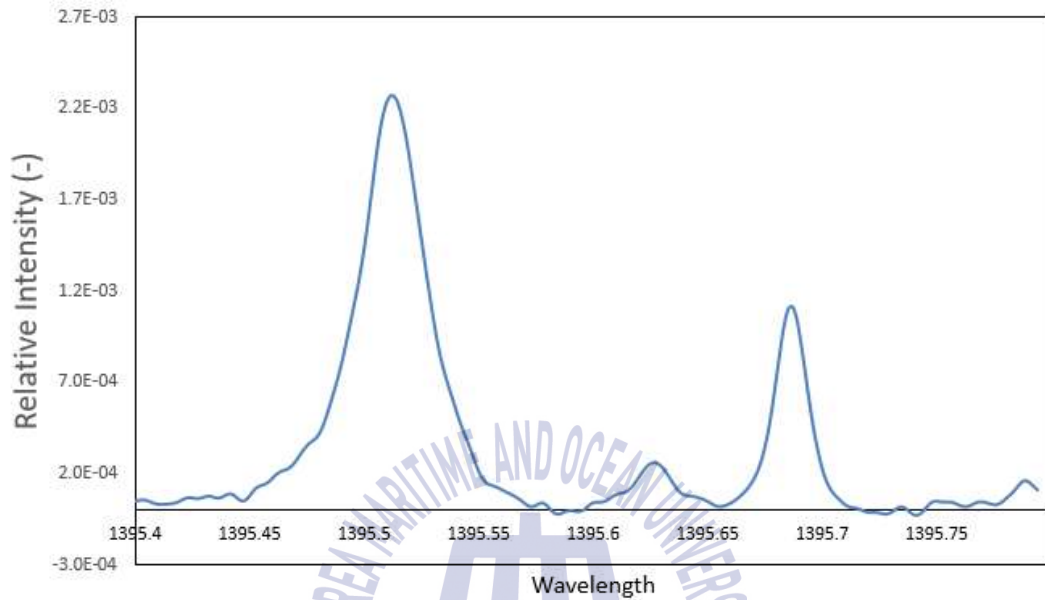


Fig. 3.7 The absorption spectrum of line number 4 measured at 1200 K

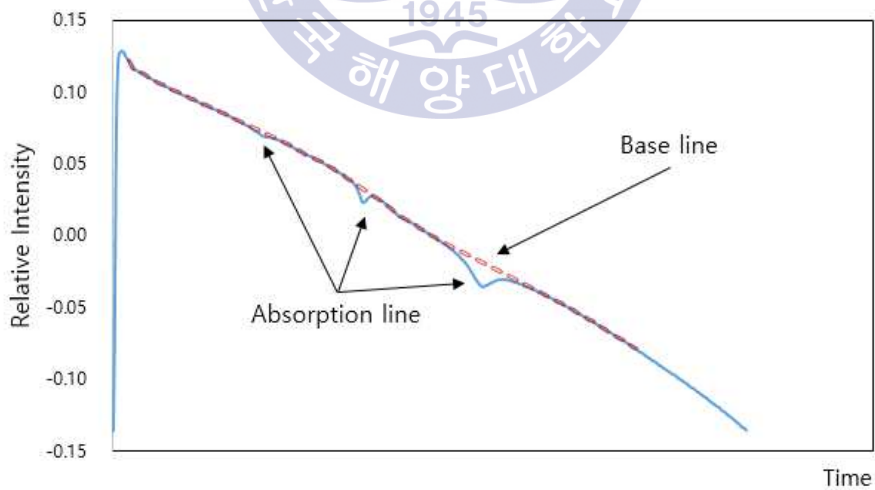


Fig. 3.8 An example of absorption line and the baseline fit

## Chapter 4 Results and Discussion

### 4.1 Comparison performance of CT-TDLAS to thermocouple

The averaged absorption lines for removing noise and the calculated absorption spectra for calibration at 300 K were illustrated in Fig. 4.1 and 4.2 respectively. The representative experimental results (at 1300 K) of averaged absorption lines and the spectra were also illustrated in Fig. 4.3 and 4.4. The measuring experiments by CT-TDLAS and thermocouple were almost simultaneously executed. The performance of CT-TDLAS was compared to the thermocouple and the results were shown in Fig. 4.5. It resultantly showed that the maximum temperature around the flame measured by CT-TDLAS was 1288 K, and in the case of thermocouple's one it was 1280 K. The difference between CT-TDLAS and thermocouple was 8 K. It was presumed this error was due to radiant heat loss of thermocouple as Fig. 3.3 showed and its inaccurate measurement position compared to the laser beam. Also, measurement itself using thermocouple affected the flow of the flame, and the flow of flame could not be always uniform, for all that the quantity of propane and dry-air for the combustion was precisely controlled by mass

flow meter. Therefore, these could be another influence factors for error. Temperature using thermocouple (R-Type) at the flame to be recorded as the highest was 1341 K which was almost same to temperature using the B-type, and it was marked as a dark blue circle in (b), Fig. 4.5.



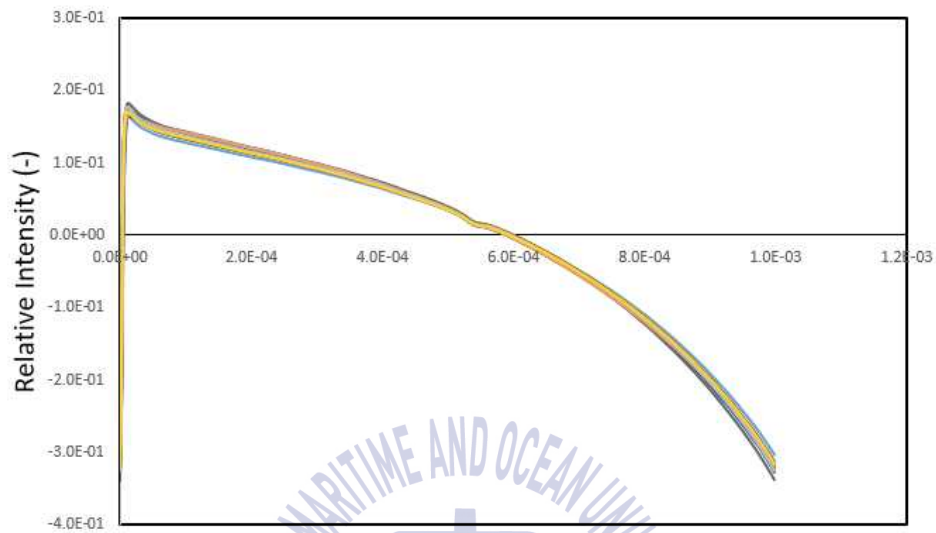


Fig. 4.1 The absorption lines at 300 K

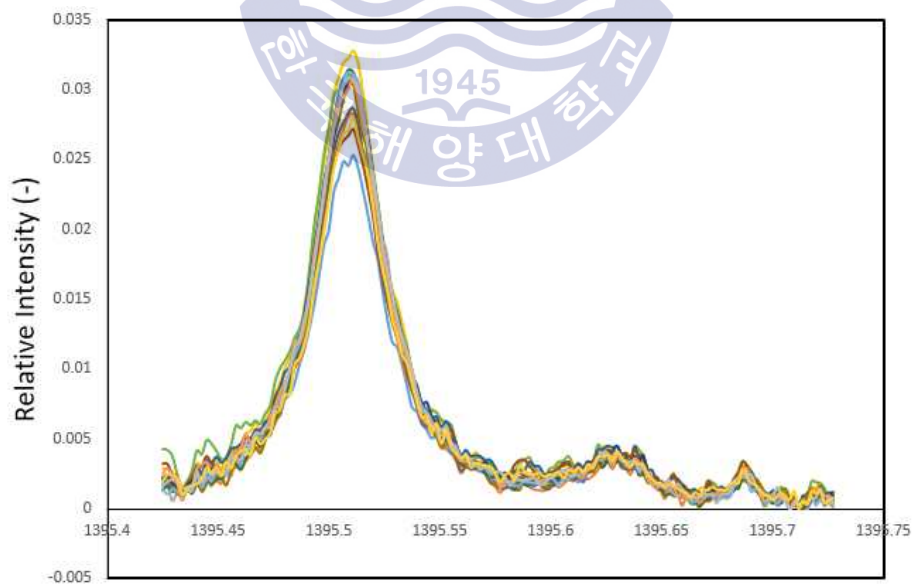


Fig. 4.2 The absorption spectra at 300 K

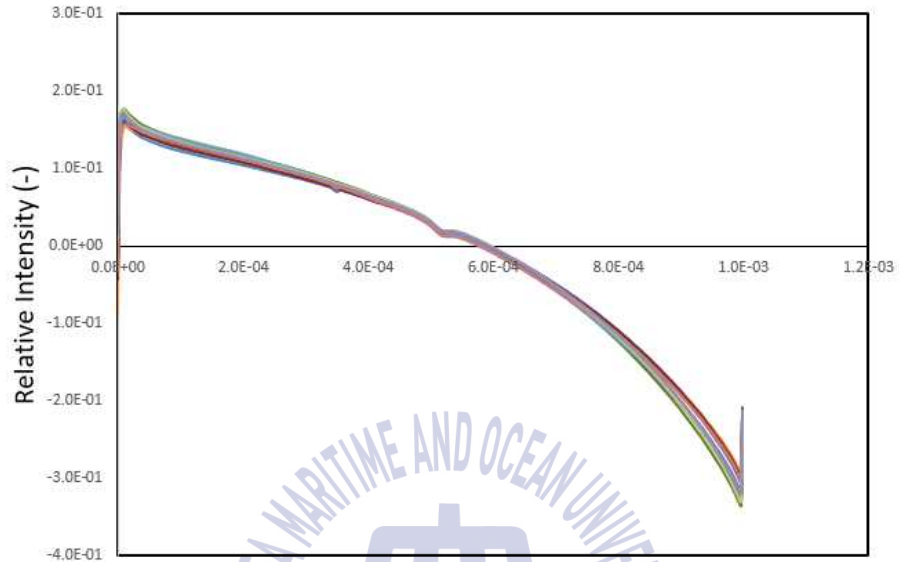


Fig. 4.3 The averaged absorption lines at 1300 K

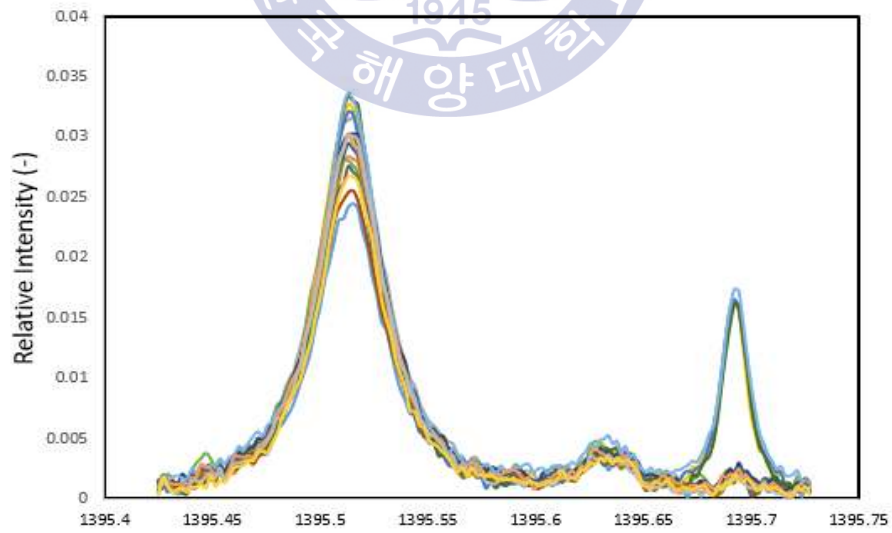
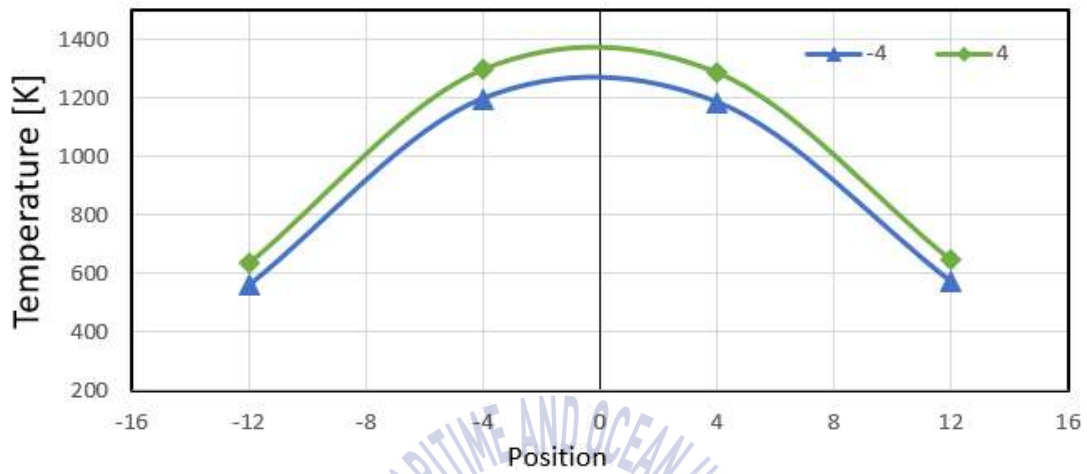
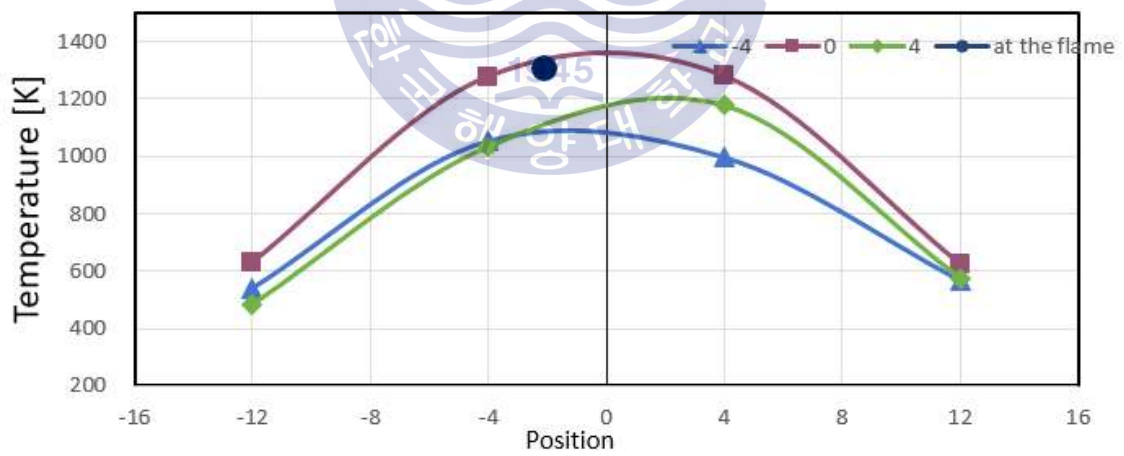


Fig. 4.4 The absorption spectra at 1300 K



(a) the results by CT-TDLAS



(b) the results by thermocouples

Fig. 4.5 Comparison of temperature results

## 4.2 Two-dimensional results using CT-TDLAS

The temperature profiles were depicted in Fig. 4.6 where red-colored rectangles were temperature information measured by thermocouple, and circle, diamond, and triangle shape were by CT-TDLAS. As tabel 3.4 presented, these CT-TDLAS results were similar to thermocouple' s one, having minor difference. And these maximum temperature were graphically depicted in Fig. 4.7. As earlier mentioned, this difference attributed to measurement error using the thermocouple. Especially, the difference was more than 100 K in the measurement around 1500 K. That was, the higher temperature the greater effect of radiation heat loss of the thermocouple.

Fig. 4.8 and 4.9 showed that temperature and concentration distributions measured using CT-TDLAS were reconstructed by the SMART method. Temperature and concentration of water vapour was high at the center where the flame was located. Since

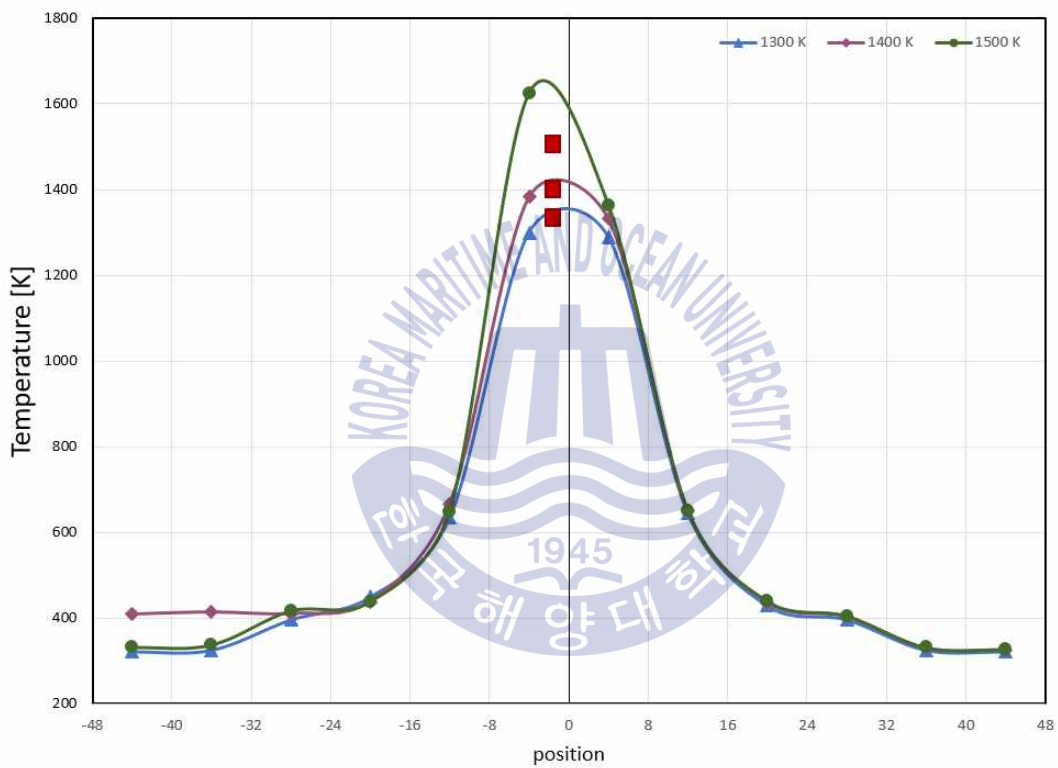
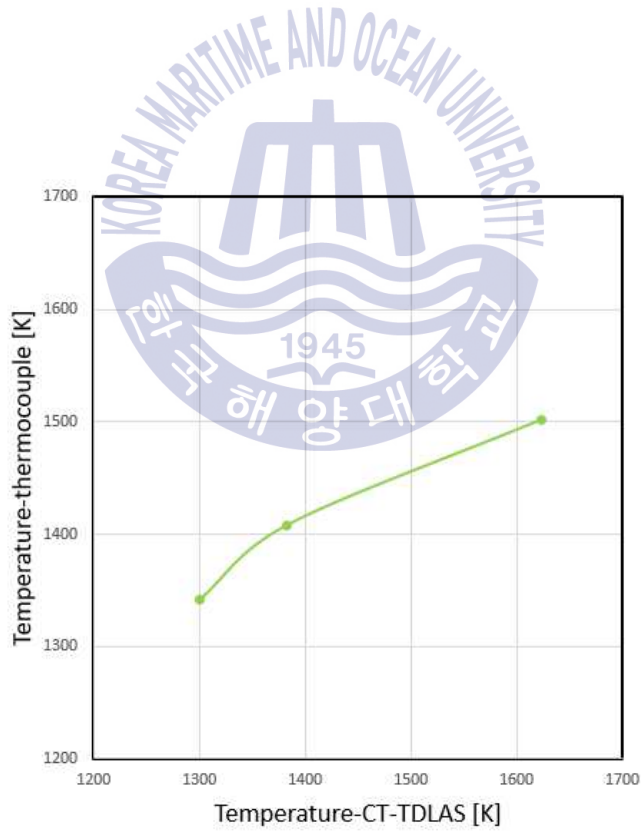


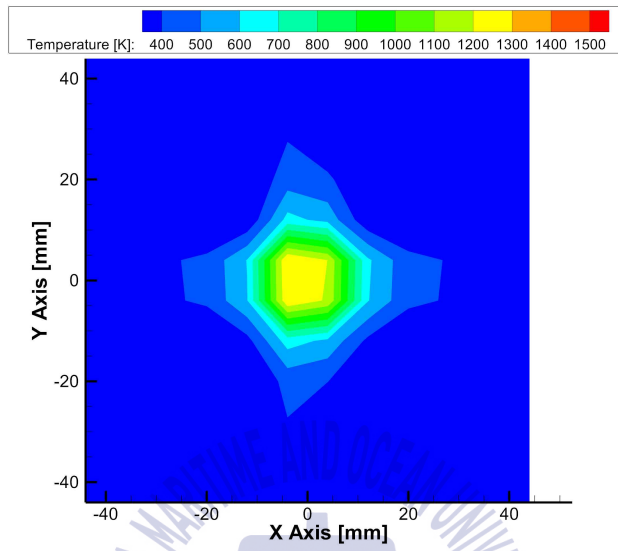
Fig. 4.6 Comparison of the temperature results I

**Table 3.4** Comparison of temperature results at 1300 K, 1400 K and 1500 K

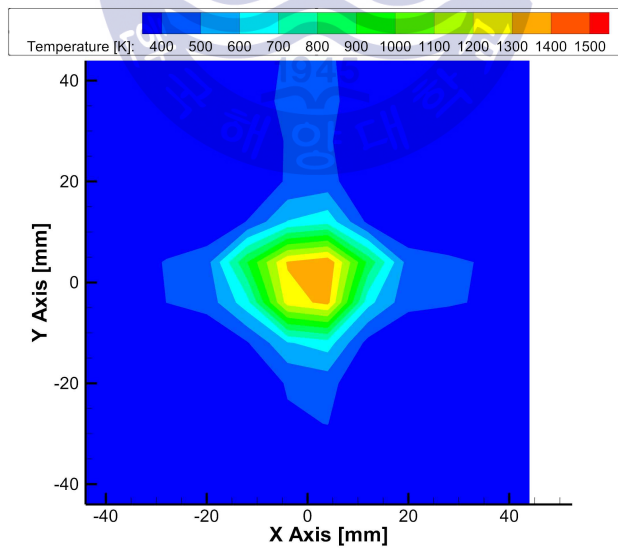
Temperature [K]	
by CT-TDLAS (y=-4)	by thermocouple (y=0)
1300	1341
1383	1408
1624	1502



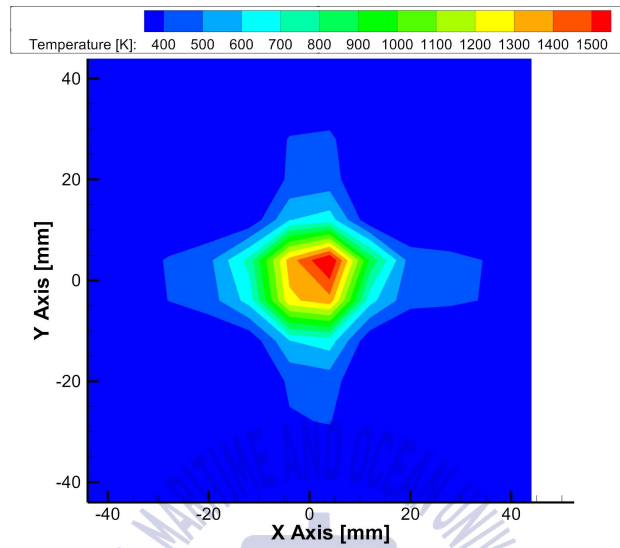
**Fig. 4.7** Comparison of the temperature results II



(a) Temperature at 1300 K

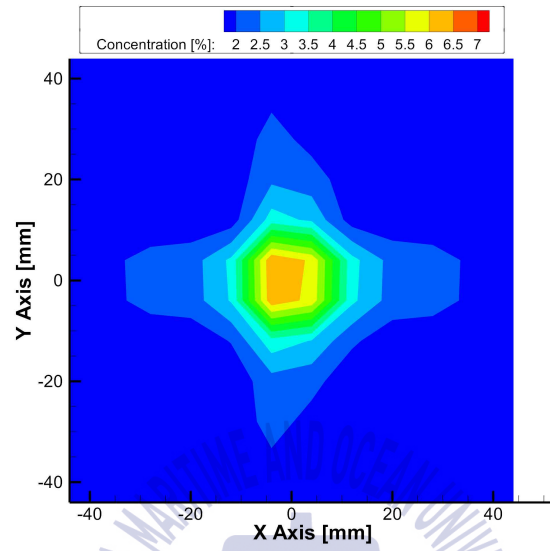


(b) Temperature at 1400 K

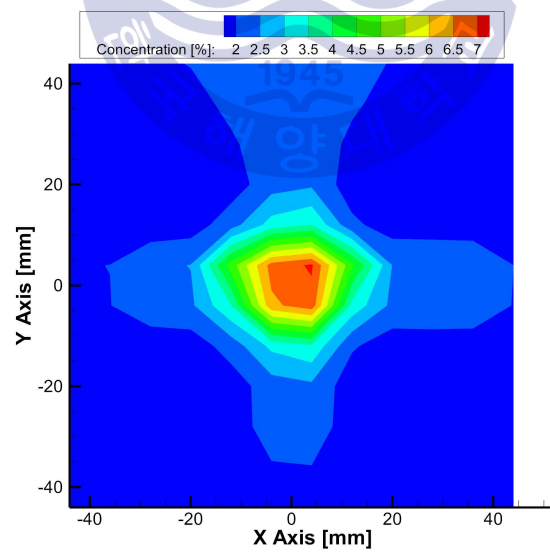


(c) Temperature at 1500 K

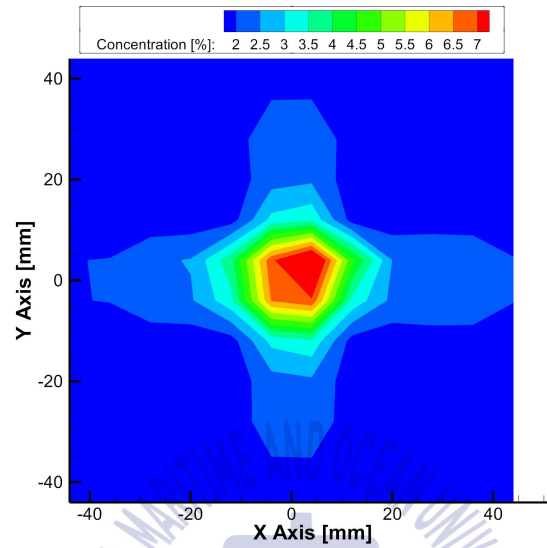
Fig. 4.8 Temperature fields by CT-TDLAS



(a) Concentration at 1300 K



(b) Concentration at 1400 K



(c) Concentration at 1500 K

Fig. 4.9 Concentration fields by CT-TDLAS

## Chapter 5 Conclusions

### 5.1 Summary

This thesis addressed to develop the measurement system called CT-TDLAS for the detecting of high temperature water-vapour. The optical experiments which measures temperature and species concentration of water-vapour in the combustion field over 1300 K using a diode laser were performed, and based on its optical signals, the two-dimensional temperature and concentration distributions were evaluated by a tomographic reconstruction algorithm, the SMART method. As a result, with CT-TDLAS the thermometry at 1300 K, 1400 K and 1500 K in the combustion fields were successfully carried out. The performance of CT-TDLAS was validated, compared to the temperature results using multiple thermocouples. The temperature difference between CT-TDLAS and thermocouples were attributed to four factors; inaccurate position and the radiant heat loss of thermocouples, non-uniform flows of flame, the shortage of laser beam at edge side for the tomographic reconstruction and the error of spectroscopic database provided by HITRAN.

## 5.2 Future works

TDLAS has been paid significant attention because of several advantages; high sensitivity, high spectral- and spatial-resolution, fast response, and non-contact measurement (X. Liu et al, 2006). However, for the practical usage of this system, a few issues below must be improved.

1. Validation: CT-TDLAS is obviously expected to be performed at higher temperature gas sensing, so that thermometry at higher temperature need be validated by thermocouple as well as other methods.

2. Fundamental spectroscopy investigations: The importance of fundamental spectroscopy research to improve HITRAN database cannot be over-emphasized, for more refined experiments and methodologies.

3. multi-laser lines: To improve the spatial resolution, blind spots in the measurements cell need to be minimized. As a solution, a octagonal structured cell with multi-laser beams is to be designed.

본 학위논문은 본인이 석사과정 동안 등재한 논문과 연구내용을 바탕으로 작성되었습니다.

## References

J.H. Kim, D.H. Doh and B.C. Choi, 2018. Evaluation of the ventilation safety requirements for the fuel gas supply system room of a gas-fueled vessel: simulated leaks of methane and propane. *Journal of Mechanical science and technology*, Vol. 32(11), pp. 5521-5532.

International Maritime Organization.

<http://www.imo.org/en/OurWork/Environment/PollutionPrevention/AirPollution/Pages/Default.aspx>

Ax, Holger, U. Stopper, W. Meier, M. Aigner, and F. Guthe. 2010. Experimental Analysis of the Combustion Behavior of a Gas Turbine Burner by Laser Measurement Techniques. *Journal of Engineering for Gas Turbines and Power*, Vol. 132, 051503, pp.1-9.

Braeuer, A., and Leipertz, A., (2009). Two-dimensional Raman mole-fraction and temperature measurements for hydrogen-nitrogen mixture analysis. *Applied optics*, Vol.48, No.4, pp.B57-B64.

Jehlickaa, J., Vitelka, P., Edwardsb, H.G.M., Heagravesb, M., and Capounc, T., (2009). Application of portable Raman instruments for fast and non-destructive detection of minerals on outcrops.

Engel, S.R., Koch, P., Braeuer, A., and Leipertz, A., (2009). Simultaneous laser-induced fluorescence and Raman imaging inside a hydrogen engine. *Applied optics*, Vol. 48, No. 35, pp.6643-6650.

X. Llu, J.B. Jeffries, R.K Honson, 2007. Measurements of spectral parameters of water-vapour transitions near 1388 and 1345 nm for accurate simulation of high-pressure absorption spectra, *measurement Science and Technology*, Vol. 18, pp 1185-1194.

Hou, H.M., Tian, Y., Li, Y., and Zheng, R.E., (2014). Study of pressure effects on laser induced plasma in bulk seawater. *Journal of Analytical Atomic Spectrometry*, Vol.29, No. 1, pp.169-175.

D.I. Yoon, J.H. Kim, M.G. Jeon, D.W. Choi, G.R. Cho, and D.H. Doh, 2018, calculating of 3-Dimensional Temperature Distribution for High- Temperature Exhaust Gas using CT-TDLAS, *The Korea Hydrogen & new energy society*, Vol. 29(1), pp. 97-104.

M.G. Jeon, Improvements of measurement technique for temperature and concentration fields using CT-TDLAS, doctoral degree thesis, Dokushima Univ., Japan.

D.F. Swinehart (1962), *Journal of Chemical Education*, The Beer-Lambert Law

L.S. Rothman, I.E. Gordon, A. Barbe, D. Chris Benner, P.F. Bernath, et al., 2008.

“The HITRAN 2008 molecular spectroscopic database” , *J. Quant. Spectrosc. Radiat. Transfer*, Vol. 110, No. 9-10, pp. 533-572.

D.I. Yoon, 2018, measurement of 3-Dimensional temperature and concentration distributions for combustion field by using CT-TDLAS, master degree thesis, Korea Maritime and Ocean Univ., Korea.

R. Gordon, R. Bender, and G.T. Herman, 1970. Algebraic reconstruction technique (ART) for three-dimensional electron microscopy and x-ray photography. *Journal of Theoretical Biology*, vol. 29, pp. 471-481.

Th.H. de Keijser et al., 1982. Use of the Voigt function in a single-line method for the analysis of X-ray diffraction line broadening, *Journal of Applied Crystallography*, Vol. 15, pp 308-314.

Y. Zaatar, J. Bechara, A. Khoury, D. Zaouk and Charles J-P. 2000. Diode laser sensor for process control and environmental monitoring, *Applied Energy*, Vol. 65, pp.107-113.

P.J. Chantry, 1971. Doppler Broadening in Beam Experiments, *Journal of chemical physics*, Vol. 55, pp.2746-2759.

Kamimoto, T., Deguchi, Y. and Kiyota, Y., 2015. High temperature field application of two dimensional temperature measurement technology using CT tunable diode laser absorption spectroscopy, *Journal of Flow Measurement and Instrumentation*,

Vol. 46, pp.51-57.

F. Wang, N.K. Cen, N. Li, J.B Jeffries, Q.X. Huang, J.H. Yan, and Y. Chi, 2010. Two-dimensional tomography for gas concentration and temperature distributions based on tunable diode laser absorption spectroscopy, *Measurement Science and Technology*, Vol. 21(4): 045301.

D. Verhoeven, 1993. Multiplicative algebraic computed tomographic algorithms for the reconstruction of multidirectional interferometric data, *Optical Engineering*, vol 32, pp. 410-419.

A.H. Andersen and A.C Kak, 1984. Simultaneous Algebraic Reconstruction Technique (SART): A Superior Implementation of the ART Algorithm, *Ultrasonic Imaging*, vol. 6, pp. 91-94.

D.C. Noll, S.J. Peltier, F.E. Boada, 1998. *Simultaneous multislice acquisition using rosette trajectories (SMART): a new imaging method for functional MRI. Magnetic Resonance in Medicine*, vol. 39, pp. 709-716.

M.G. Jeon, Y. Deguchi, T. Kamimoto, D. H. Doh, and G. R. Cho, 2017. Performances of new reconstruction algorithms for CT-TDLAS (computer tomography-tunable diode laser absorption spectroscopy, *Applied Thermal Engineering*, Vol. 115, pp. 1148-1160.

M.G. Jeon, 2014, Improvements of Tomographic Quantification Technique for

Temperature and Concentration Fields using a Multiple Algebraic Reconstruction Techniques, *Experiments in Fluids*, pp. 553-568.

Y. Deguchi, 2013. Two Dimensional Temperature Measurement Using CT Tunable Laser Diode Absorption Spectroscopy, *Journal of the Combustion Society of Japan*, Vol. 55, pp.249-254.

E.E. Whiting, 1968. An empirical approximation to the voigt profile, *Journal of Quantitative Spectroscopy and Radiative Transfer*, Vol. 8, pp. 1379-1384.

L. Dong, C. Li, N.P. Sanchez, A.K. Gluszek, R.J. Griffin, and F.K. Tittel, 2016. Compact CH<sub>4</sub> sensor system based on a continuous-wave, low power consumption, room temperature interband cascade laser, *Applied Physics letters*, Vol. 108, no. 1.

I. Kojima, M. Kurahashi. 1987. Application of asymmetrical Gaussian/Lorentzian mixed function for X-ray photoelectron curve synthesis, *Journal of Electron Spectroscopy and Related Phenomena*, vol.42, Issue 2

X. Liu, 2006, Line-of-sight absorption of H<sub>2</sub>O vapor: gas temperature sensing in uniform and non uniform flows, Doctoral degree thesis, Stanford Univ., USA.

(text book)

A. Yariv, An introduction to theory and applications of quantum mechanics, Wiley, NY, 1982.

C.N. Banwell and E.M. McCash, Fundamentals of molecular spectroscopy, 4th edition, McGraw-Hill Book Co., Maidenhead, Berkshire, 1994.

G. Herzberg, Molecular spectra and molecular structure II: Infrared and Raman spectra of polyatomic molecules, Van Nostrand Reinhold, NY, 1945, Reprinted Krieger Malabar Publishing, FL, 1991.

R.k. Hanson, R.M. Spearrin, C.S. Goldenstein. Spectroscopy and Optical Diagnostics for Gases, Springer. 2010.

Y. Deguchi, Industrial Applications of Laser Diagnostics, CRC Press, 2012.